SCIENCE CHINA Materials ARTICLES

mater.scichina.com link.springer.com

Published online 22 June 2021 | https://doi.org/10.1007/s40843-021-1678-y
Sci China Mater 2021, 64(11): 2729–2738

Regulating the electronic structure of NiFe layered double hydroxide/reduced graphene oxide by Mn incorporation for high-efficiency oxygen evolution reaction

Binbin Jiang[1,3†], Weng-Chon Cheong[2,4†], Renyong Tu[2], Kaian Sun[2], Shoujie Liu[5], Konglin Wu[1*], Hengshuai Shang[1], Aijian Huang[6*], Miao Wang[1], Lirong Zheng[7], Xianwen Wei[1] and Chen Chen[2*]

ABSTRACT **The development of highly efficient and cost-effective oxygen evolution reaction (OER) electrocatalysts for renewable energy systems is vitally essential. Modulation of the electronic structure through heteroatom doping is considered as one of the most potential strategies to boost OER performances. Herein, a rational design of Mn-doped NiFe layered double hydroxide/reduced graphene oxide (Mn-NiFe LDH/rGO) is demonstrated by a facile hydrothermal approach, which exhibits outstanding OER activity and durability. Experimental results and density functional theory (DFT) calculations manifest that the introduction of Mn can reprogram the electronic structure of surface active sites and alter the intermediate adsorption energy, consequently reducing the potential limiting activation energy for OER. Specifically, the optimal Mn-NiFe LDH/rGO composite shows an enhanced OER performance with an ultralow overpotential of 240 mV@10 mA cm^{-2}, Tafel slope of 40.0 mV dec^{-1} and excellent stability. Such superior OER activity is comparable to those of the recently reported state-of-the-art OER catalysts. This work presents an advanced strategy for designing electrocatalysts with high activity and low cost for energy conversion applications.**

Keywords: Mn, NiFe layered double hydroxides, electrocatalysts, oxygen evolution reaction, DFT calculations

INTRODUCTION

Oxygen evolution reaction (OER) is a critical process for the renewable energy systems [1–3]. However, the OER suffers from the sluggish kinetic process due to the multiple electron transfer [4,5]. Therefore, the rational design and construction of efficient electrocatalysts to boost the OER process are highly desirable for the sustainable energy systems. Generally, Ir- and Ru-based nanomaterials are considered as the benchmark electrocatalysts for OER to date, but the scarcity and high cost limit their commercial applications in large scale [6–9]. Thus, developing highly efficient electrocatalysts based on earth-abundant metals represents a promising alternate to reduce the consumption of precious metals and many research efforts have been devoted to this field [10–13].

Recently, layered double hydroxides (LDHs) have exhibited remarkably potential applications in designing advanced OER electrocatalysts [14–19]. For example, NiFe LDH displayed enhanced OER performance in alkaline solutions [20,21] and the improvement of activity was generally attributed to the high oxidation state of Fe during the OER process [22,23]. Nevertheless, compared with other LDHs systems, NiFe LDHs usually possess a weak binding energy of *O on the active sites, which is

[1] Institute of Clean Energy and Advanced Nanocatalysis (iClean), School of Chemistry and Chemical Engineering, Anhui University of Technology, Maanshan 243002, China
[2] Department of Chemistry, Tsinghua University, Beijing 100084, China
[3] Anhui Key Laboratory of Functional Coordination Compounds, Anqing Normal University, Anqing 246011, China
[4] Department of Physics and Chemistry, Faculty of Science and Technology, University of Macau, Macao, China
[5] Chemistry and Chemical Engineering of Guangdong Laboratory, Shantou 515063, China
[6] School of Electronics Science and Engineering, University of Electronic Science and Technology of China, Chengdu 610054, China
[7] Beijing Synchrotron Radiation Facility (NSRF), Institute of High Energy Physics, Chinese Academy of Sciences, Beijing 100049, China
† These authors contributed equally to this work.
* Corresponding authors (emails: klwuchem@ahut.edu.cn (Wu K); 201811022517@std.uestc.edu.cn (Huang A); cchen@mail.tsinghua.edu.cn (Chen C))

unfavorable for the OER process [24]. Thus, designing an effective NiFe LDH catalyst to break the theoretical limitation is of great significance yet challenging.

On the other hand, previous reports indicated that the intrinsic activity of LDH can be improved by doping with third metals (Al, V, Cr, Ce, and Mo) to modulate the electronic structure of surface atoms [25–29]. For example, Jin and coworkers [30] reported that the NiFeCr LDH exhibited an exceptionally high electrocatalytic activity with an overpotential of 225 mV to reach 10 mA cm^{-2} due to the dopant of Cr. In addition, the theoretical calculation revealed that the Co-doped NiFe LDH can decrease the energy barrier for the formation of OOH*, thus accelerating the OER kinetics [31]. Inspired by the above achievements, we explore the incorporation of other dopants into NiFe LDH to adjust the energy barrier for the adsorption of oxygen intermediates during OER.

Herein, we demonstrate that the Mn-doped NiFe LDH/reduced graphene oxide (Mn-NiFe LDH/rGO) exhibits an outstanding OER performance with a low overpotential to reach 10 mA cm^{-2} (240 mV), a small Tafel slope of 40.0 mV dec^{-1} and remarkable stability in 1.0 mol L^{-1} KOH. The density functional theory (DFT) calculations reveal that the Mn dopant in the Mn-NiFe LDH/rGO can modulate the electronic structure of Fe active site and reduce the energy barrier in OER reaction, which can break up the scaling relationships of oxygen intermediates and accelerate the OER kinetics. This work presents a feasible synthetic approach to construct highly active and durable OER electrocatalysts, which will not only pave an avenue for the future study of the layered hydroxide composites, but also promote the development of earth-abundant metal-based materials for energy conversion and storage.

EXPERIMENTAL SECTION

Synthesis of Mn-NiFe LDH/rGO

Mn-NiFe LDH/rGO was prepared *via* a simple hydrothermal reaction. Specifically, the rGO was firstly obtained through the chemical reduction of graphene oxide (Supplementary information, SI). After that, 5.0 mg of rGO was dispersed in 10 mL of ethylene glycol with the aid of ultrasonication. Then, 10 mL of water solution containing $NiCl_2{\cdot}6H_2O$, $FeCl_3{\cdot}6H_2O$ and $MnCl_2{\cdot}4H_2O$ (the molar ratio of Ni, Fe and Mn is 50:15:3, and the total concentration of metal is 0.262 mmol L^{-1}) was added dropwise into the above rGO solution under stirring. After being continuously stirred for 5 h, 100 mg of urea was introduced into the above mixed solution. Subsequently, the as-obtained homogeneous solution was transferred into a 25-mL Teflon-lined stainless-steel autoclave and heated at 120°C for 12 h. The resulting product (denoted as *x* Mn-NiFe LDH/rGO, where the *x* is the molar content of the doped Mn) was washed with distilled water and absolute ethanol, and then dried in a vacuum oven for further characterization. Other mass contents of doped Mn-NiFe LDH/rGO, NiFe LDH/rGO, and Mn-NiFe LDH were also prepared with the similar procedures.

Characterization

Structures and morphologies of the samples were characterized by powder X-ray diffraction (XRD), scanning electron microscopy (SEM), and transmission electron microscopy (TEM). Elemental mapping images were characterized by energy-dispersive X-ray spectrometry (EDS) attached on FEI Tecnai F20 TEM. Chemical states of the samples were analyzed by X-ray photoelectron spectroscopy (XPS). The Fe K-edge and Ni K-edge were obtained from Beijing Synchrotron Radiation Facility (BSRF). The detailed characterization conditions are shown in SI.

Electrochemical measurements

All electrochemical measurements were tested by a CHI 760 E electrochemical workstation *via* the three-electrode systems, and the detailed testing methods and measurement conditions are shown in SI.

DFT calculations

All calculations were performed by means of spin polarized DFT methods using the Vienna *Ab initio* Simulation Package (VASP), and the detailed DFT calculation methods and process are shown in SI.

RESULTS AND DISCUSSION

XRD evidences that there is no sign of other characteristic peaks after Mn doping compared with that of the original NiFe LDH/rGO (Fig. 1a), suggesting a small amount of Mn dopant will not destroy the crystalline structure of NiFe LDH/rGO. The morphologies of NiFe LDH/rGO, Mn-NiFe LDH and Mn-doped NiFe LDH/rGO were characterized by SEM and TEM images (Fig. S1, and Fig. 1b, c), which confirmed that 5.0 Mn-NiFe LDH/rGO retained the original shape of nanosheets after the Mn doping. High-resolution TEM (HRTEM) image displays the crystallinity of 5.0 Mn-NiFe LDH/rGO (Fig. 1d) and the spacings of the lattice fringes of 0.19 (Fig. 1e) and 0.33 nm (Fig. 1f) are assigned to the (018) plane of NiFe

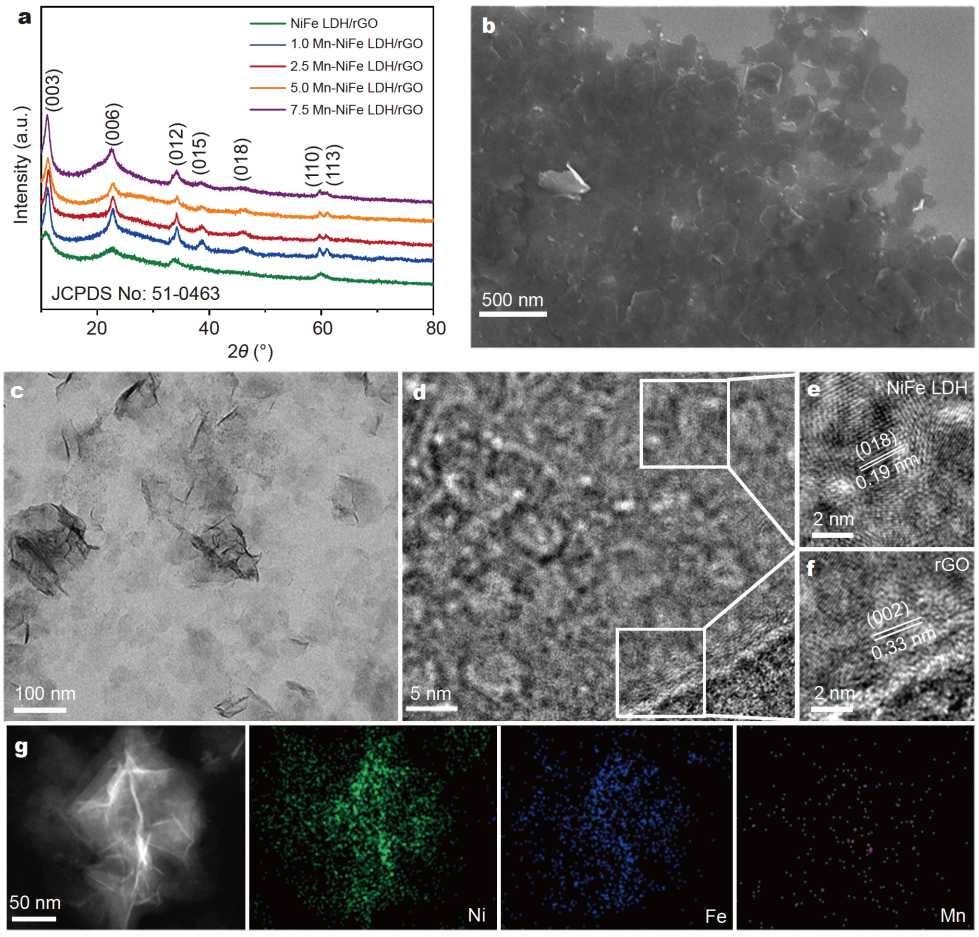

Figure 1 Morphology and structural characterization of NiFe LDH/rGO and Mn-doped NiFe LDH/rGO. (a) The XRD patterns of NiFe LDH/rGO, 1.0 Mn-NiFe LDH/rGO, 2.5 Mn-NiFe LDH/rGO, 5.0 Mn-NiFe LDH/rGO and 7.5 Mn-NiFe LDH/rGO; (b) SEM, (c) TEM, (d) HRTEM images of 5.0 Mn-NiFe LDH/rGO. The enlarged areas denoted in (d) correspond to the HRTEM images of (e) NiFe LDH and (f) rGO, respectively. (g) HADDF-STEM image and corresponding EDS mapping of 5.0 Mn-NiFe LDH/rGO.

LDH and the (002) plane of rGO, respectively. In addition, the high angle annular dark field scanning TEM (HAADF-STEM) and the corresponding EDS images evidence that a small amount of Mn is homogeneously distributed throughout the entire materials (Fig. 1g and Fig. S2), suggesting that the Mn doping in NiFe LDH/rGO system has been successfully achieved.

The oxidation state of surface and electronic structure of Mn-doped NiFe LDH/rGO and NiFe LDH/rGO were investigated by XPS. The full scan spectra (Fig. S3) reveal that the 5.0 Mn-NiFe LDH/rGO is composed of Ni, Fe, Mn, C and O elements, which is consistent with the EDS mapping (Fig. 1g). As shown in Fig. 2a, the Mn 2p peak is deconvoluted into four peaks. The peaks located at binding energies of 641.7 and 653.3 eV correspond to Mn $2p_{1/2}$ and Mn $2p_{3/2}$, confirming the existence of Mn^{3+} in the 5.0 Mn-NiFe LDH/rGO [32]. While the hydroxyl ion is a weak-field ligand, the Mn^{3+} ions in bimetallic LDH are shown in a high spin state, which will result in lattice instability in LDH composite [17]. Therefore, the Mn^{3+} can be easily oxidized to Mn^{4+}, and thus the peaks of Mn (IV) can be observed in the Mn 2p XPS spectra. The incorporation of metal can modulate the electronic structure of active sites [12,22], improving the electrocatalytic activity. Consequently, after Mn doping, the peak of Fe $2p_{3/2}$ in 5.0 Mn-NiFe LDH/rGO shifts 0.4 eV lower relative to that of the NiFe LDH/rGO (Fig. 2b). Additionally, the binding energy of Ni $2p_{3/2}$ of 5.0 Mn-NiFe LDH/rGO also shifts negatively for ~0.5 eV against that of the NiFe LDH/rGO (Fig. 2c). XPS fitting shows that the peaks of 712.2 and 724.8 eV are attributed to Fe $2p_{3/2}$ and Fe $2p_{1/2}$, respectively, in 5.0 Mn-NiFe LDH/rGO, indicating the presence of Fe^{3+} [17]. Another two peaks belong to the Fe satellite (Fig. 2b). For the Ni 2p

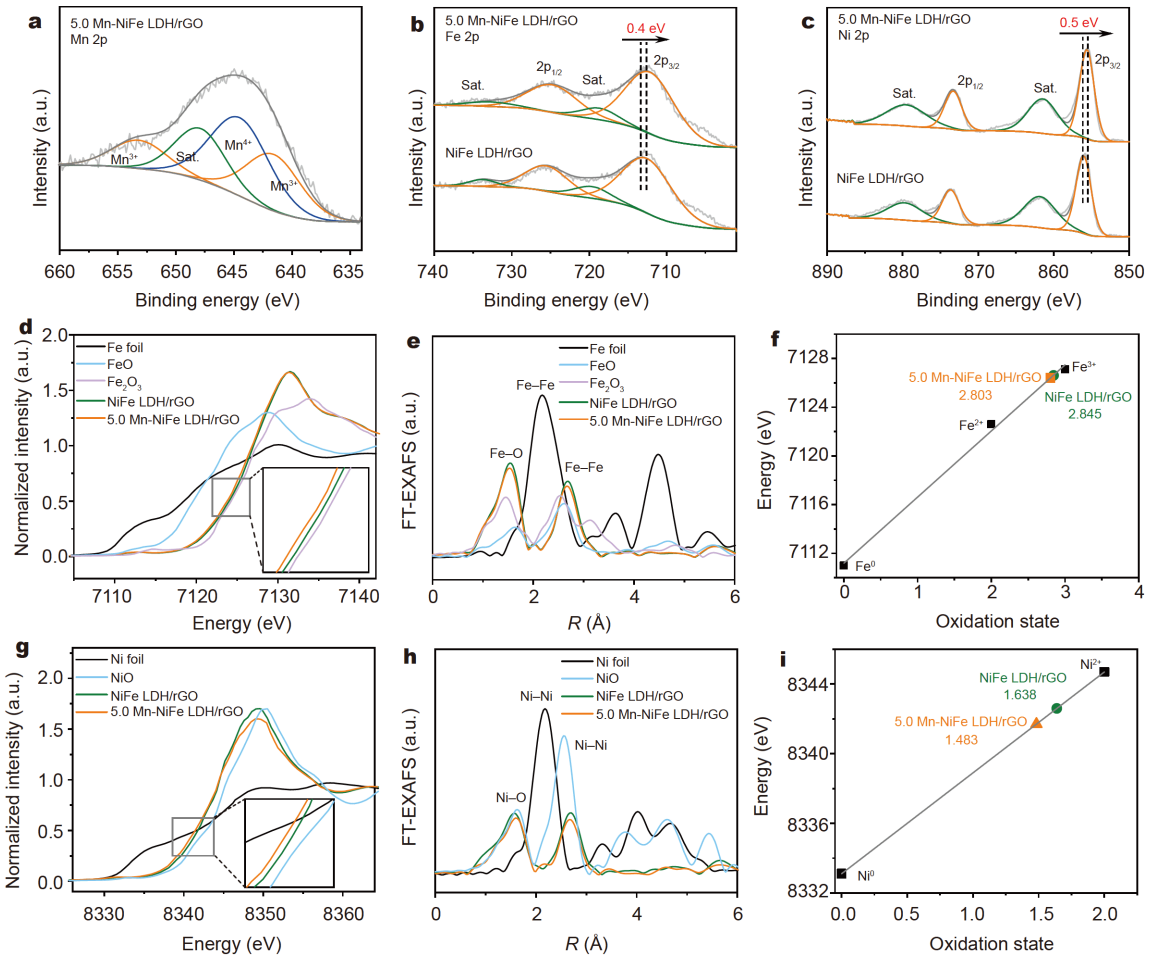

Figure 2 XPS and XAS analyses of NiFe LDH/rGO and Mn-doped NiFe LDH/rGO. The high-resolution XPS spectra of (a) Mn 2p, (b) Fe 2p and (c) Ni 2p of 5.0 Mn-NiFe LDH/rGO; (d) Fe K-edge XANES spectra; (e) magnitude of k^3-weighted Fourier transforms of Fe K-edge EXAFS spectra of Fe foil, FeO, Fe_2O_3, NiFe LDH/rGO and 5.0 Mn-NiFe LDH/rGO; (f) oxidation states of Fe in the NiFe LDH/rGO and 5.0 Mn-NiFe LDH/rGO; (g) Ni K-edge XANES spectra; (h) magnitude of k^3-weighted Fourier transforms of Ni K-edge EXAFS spectra of Ni foil, NiO, NiFe LDH/rGO and 5.0 Mn-NiFe LDH/rGO; and (i) oxidation states of Ni in the NiFe LDH/rGO and 5.0 Mn-NiFe LDH/rGO.

spectra, peaks at binding energies of 855.6 and 873.3 eV are assigned to Ni $p_{3/2}$ and Ni $p_{1/2}$ of Ni (II), while the two peaks at 861.4 and 879.5 eV correspond to the Ni satellite (Fig. 2c) [33]. Moreover, three peaks at 530.8, 532.5, and 533.6 eV are clearly observed from the O 1s spectra (Fig. S4), which correspond to metal-oxide bond, C=O and adsorbed water, respectively.

X-ray absorption near-edge structure (XANES) and extended X-ray absorption fine structure (EXAFS) were performed to characterize the precise electronic structures of Fe and Ni in 5.0 Mn-NiFe LDH/rGO. From the Fe K-edge XANES spectra (Fig. 2d), the absorption edge of Fe K-edge in 5.0 Mn-NiFe LDH/rGO shifted to lower energy compared with NiFe LDH/rGO due to the Mn dopant, suggesting a slight decrease in the Fe oxidation state after the introduction of Mn in 5.0 Mn-NiFe LDH/rGO. The first derivative can be more intuitive to characterize the change of metal oxidation state based on the absorption threshold energy (E_0) [34,35]. According to the first derivatives of the Fe K-edge XANES spectra, the first maxima E_0 is 7111, 7122.6, 7127.1, 7126.6, and 7126.4 eV for Fe foil, FeO, Fe_2O_3, NiFe LDH/rGO, and 5.0 Mn-NiFe LDH/rGO (Fig. S5), respectively. Based on the Fe K-edge XANES spectra, the fitting average oxidation states are shown in Fig. 2f. The average valence state of Fe in the 5.0 Mn-NiFe LDH/rGO is about +2.803, which is slightly lower than that of Fe in NiFe LDH/rGO (+2.845).

The R-space spectra (Fig. 2e) exhibit that the peak intensity of 5.0 Mn-NiFe LDH/rGO is slightly lower than that of the NiFe LDH/rGO, which is attributed to the increase of disorder degree around Fe caused by Mn

doping. Moreover, the Ni K-edge XANES spectra and Ni K-edge FT EXAFS were also conducted to reveal the Ni structure in 5.0 Mn-NiFe LDH/rGO (Fig. 2g and h), displaying a trend similar to that of Fe. According to the first derivatives of the Ni K-edge XANES spectra, the first maxima E_0 is 8333.1, 8344.7, 8342.6, and 8341.7 eV for Ni foil, NiO, NiFe LDH/rGO, and 5.0 Mn-NiFe LDH/rGO (Fig. S6), respectively. The fitting average oxidation states show that the average valence state of Ni in the 5.0 Mn-NiFe LDH/rGO is about +1.483 (Fig. 2i), which is lower than that of Ni in NiFe LDH/rGO (+1.638). Then, the products of NiFe LDH/rGO and 5.0 Mn-NiFe LDH/rGO were characterized by Auger electron spectroscopy (AES, Fig. S7). The results also show that the kinetic energies of Fe (Fig. S7a) and Ni (Fig. S7b) shift to high energy after Mn doping, which indicates that the valence states of Ni and Fe decrease [36]. Here, when Mn is doped, the effects on the oxidation states of Ni and Fe are different, which may be caused by the difference in electronegativities of Mn, Ni, and Fe [36,37], and the induction effect of high-valent Mn on Ni and Fe [38]. Thereby, the above analyses indicate that Mn dopant can modulate the electronic properties of Fe and Ni in 5.0 Mn-NiFe LDH/rGO.

The OER electrocatalytic activity of the as-prepared catalysts was evaluated in the oxygen-saturated 1.0 mol L^{-1} KOH with 95% *iR* compensation and all the potentials were referenced to a reversible hydrogen electrode (RHE) (SI for more details). The peak around 1.43 V of the as-prepared composites is assigned to the Ni(II)/Ni(III or IV) redox process in alkaline environment (Fig. 3a and b) [39]. Compared with the NiFe LDH/rGO, the Mn-NiFe LDH/rGO exhibits higher current density at given applied potentials. To be specific, the 5.0 Mn-NiFe LDH/rGO displays the lowest overpotential (240 mV) to achieve the current density of 10 mA cm^{-2}, which is superior to that of NiFe LDH/rGO (293 mV), 1.0 Mn-NiFe LDH/rGO (268 mV), 2.5 Mn-NiFe LDH/rGO (261 mV) and 7.5 Mn-NiFe LDH/rGO (274 mV). In addition, the overpotential of 5.0 Mn-NiFe LDH/rGO to deliver 10 mA cm^{-2} is also lower than that of Mn-NiFe LDH (278 mV), Ni LH/rGO (450 mV), NiFe LDH/rGO (293 mV) and RuO_2 (370 mV) (Fig. 3b). Moreover, the OER activity of 5.0 Mn-NiFe LDH/rGO also surpasses other reported advanced LDH catalysts, including the NiCoFe-LDH HP (276 mV@10 mA cm^{-2}) [40], GCN/$Ni(OH)_2$ (290 mV@10 mA cm^{-2}) [41], ZnNi LDH/N-rGO (290 mV@10 mA cm^{-2}) [42], $Ni_{0.75}V_{0.25}$ LDH (310 mV@10 mA cm^{-2}) [43], NP Au/Cr-NiFe (323 mV@10 mA cm^{-2}) [32], and 3D NiFe-LDH HMS (290 mV@10 mA cm^{-2}) [44].

Tafel slope is an intrinsic activity derived from the corresponding linear sweep voltammetry (LSV) curves of a catalyst [39]. As shown in Fig. 3c, the 5.0 Mn-NiFe LDH/rGO shows the lowest Tafel slope (40.0 mV dec^{-1}) among all the as-prepared composites and is even comparable to the recently reported advanced OER electrocatalysts under similar conditions (Table S1), such as Ni-Fe LDH (49.4 mV dec^{-1}) [20], NiCoFe-LDH HP (56 mV dec^{-1}) [40], GCN/$Ni(OH)_2$ (77 mV dec^{-1}) [41], $Ni_{0.75}V_{0.25}$ LDH (50 mV dec^{-1}) [43], 3D NiFe-LDH HMS (51 mV dec^{-1}) [44], and $TiO_2C@CN_{x,950}$ (69 mV dec^{-1}) [45], which suggests the most favorable OER kinetics of 5.0 Mn-NiFe LDH/rGO.

The electrochemical active surface area (ECSA) is an important factor for an electrocatalyst, and the larger ECSA is beneficial for the electrocatalytic activity [46,47]. Fig. S8 shows the CV curves of 5.0 Mn-NiFe LDH/rGO, NiFe LDH/rGO, Mn-NiFe LDH and RuO_2 with different scan rates in 1.0 mol L^{-1} KOH. The double-layer capacitance (C_{dl}) can be achieved by plotting the $\Delta J/2$ ($=1/2(J_a - J_c)$) at 1.2 V *versus* the scan rate, and the C_{dl} is proportional to the ECSA [47]. The C_{dl} of 5.0 Mn-NiFe LDH/rGO is 5.7 mF cm^{-2}, which is 2.4, 3.2 and 4.1 times that of Mn-NiFe LDH, NiFe LDH/rGO and RuO_2, respectively (Fig. 3d), indicating that 5.0 Mn-NiFe LDH/rGO has a larger electroactive surface area, which enhances the OER performance. Additionally, electrochemical impedance spectroscopy (EIS) was performed at the overpotential of 285 mV to evaluate the intrinsic conductivity for catalysts. The equivalent circuit is fitted by a $R_s-(R_1||CPE_1)-(R_{ct}||CPE_2)$ model (inset Fig. 3e), where R_s is the solution resistance, $R_1||CPE_1$ is related to the porosity of electrode surface and the $R_{ct}||CPE_2$ corresponds to the kinetics of the OER. Fig. 3e and Fig. S9 display that the 5.0 Mn-NiFe LDH/rGO exhibits smaller R_{ct} (27.4 Ω) than Mn-NiFe LDH (40.7 Ω), NiFe LDH/rGO (71.4 Ω) and RuO_2 (689.0 Ω), suggesting that a much faster charge-transfer rate due to the dopant of Mn, resulting in the remarkable electrocatalytic activity for OER [48,49], which is in good agreement with the result of the Tafel slope. These results indicate that Mn dopant can improve the intrinsic property of the electrocatalyst.

The stabilities of the 5.0 Mn-NiFe LDH/rGO, NiFe LDH/rGO and RuO_2 were performed by a chronopotentiometry measurement at 10 mA cm^{-2}. As shown in Fig. 3f, the overpotential of 5.0 Mn-NiFe LDH/rGO displays a slight increase about 5 mV after 72,000 s constant test. Nevertheless, the overpotential of NiFe LDH/rGO and RuO_2 both increase 12 mV. Furthermore, the XPS and TEM were employed to investigate the stability

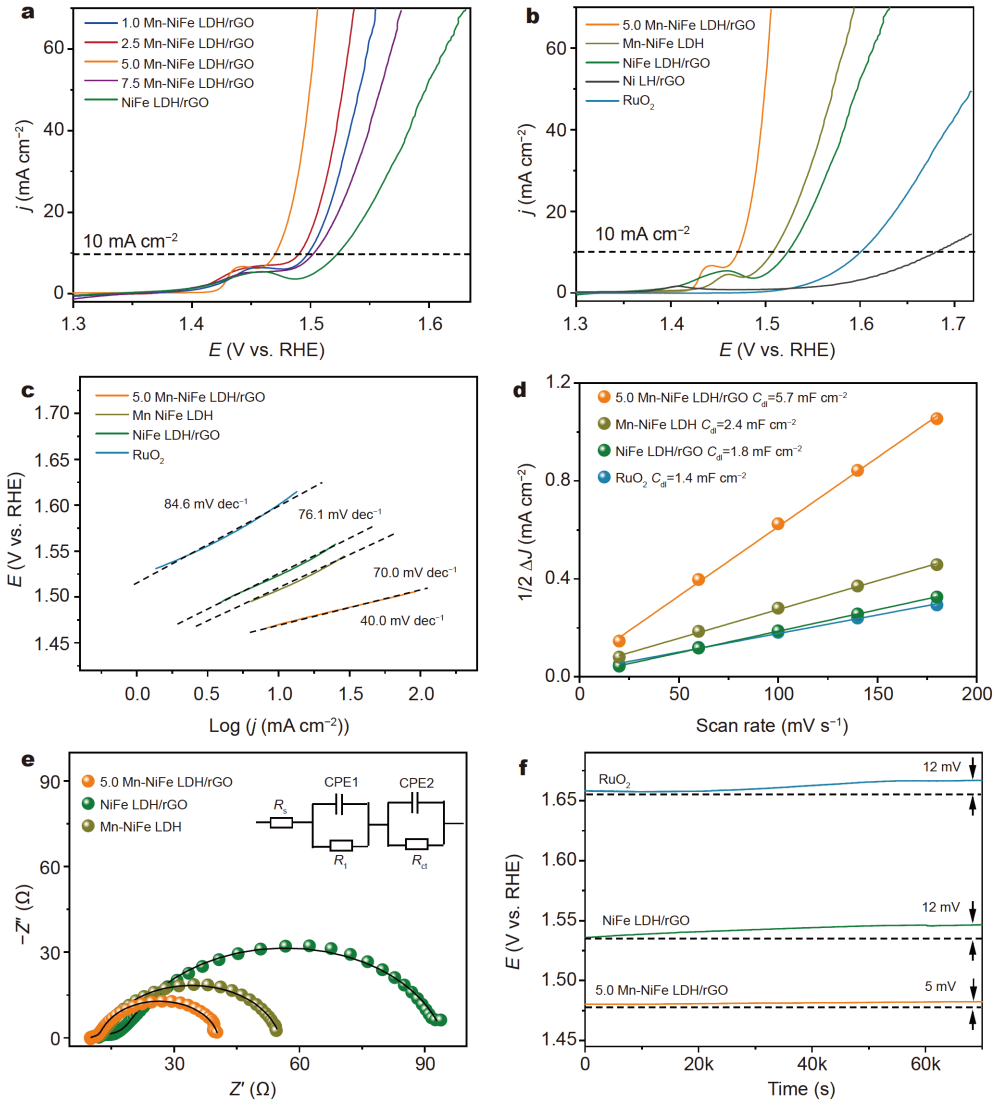

Figure 3 Electrocatalytic performance of NiFe LDH/rGO and Mn-doped NiFe LDH/rGO for OER. (a) The LSV curves of different Mn-doped NiFe/rGO with 95% *iR* corrected in the O_2-saturated 1.0 mol L^{-1} KOH; (b) the LSV curves of 5.0 Mn-NiFe LDH/rGO, RuO_2, NiFe LDH/rGO, Mn-NiFe LDH and Ni LH/rGO with 95% *iR* corrected in the O_2-saturated 1.0 mol L^{-1} KOH; (c) Tafel slope derived from the (b); (d) C_{dl} values at different scan rates (1.20 V *vs.* RHE); (e) Nyquist plots of 5.0 Mn-NiFe LDH/rGO, NiFe LDH/rGO and Mn-NiFe LDH in 1.0 mol L^{-1} KOH at the overpotential of 285 mV; (f) stability of 5.0 Mn-NiFe LDH/rGO, NiFe LDH/rGO and RuO_2 at the current density of 10 mA cm^{-2}. The inset in Fig. 3e is the equivalent circuit.

of 5.0 Mn-NiFe LDH/rGO. The peak positions of Fe 2p and Ni 2p without obvious change after the stability test indicate great chemical stability of 5.0 Mn-NiFe LDH/rGO (Fig. S10). The morphology of 5.0 Mn-NiFe LDH/rGO remains unchanged after the electrochemical analysis (Fig. S11), highlighting the excellent structural integrity for Mn-doped NiFe LDH/rGO in alkaline media.

To deeply understand the mechanism of the enhanced water oxidation activity, DFT+U calculations were employed to systematically investigate the intermediate binding energies and reaction overpotential of the NiFe LDH/rGO and Mn-NiFe LDH/rGO. The reaction pathways were proposed based on the following mechanism [50]:

Step 1: $H_2O(l) + 2^* \rightarrow {}^*{+}{}^*OH + H^+ + e^-$; $\Delta G1$

Step 2: $^*OH + {}^* \rightarrow {}^*{+}{}^*O + H^+ + e^-$; $\Delta G2$

Step 3: $^*O + {}^*{+}H_2O(l) \rightarrow {}^*OOH + H^+ + e^-$; $\Delta G3$

Step 4: $^*OOH \rightarrow O_2(g) + H^+ + e^-$; $\Delta G4$

where "*" represents the active site on the surface of NiFe LDH and Mn-NiFe LDH. "*OH", "*O" and "*OOH" are the adsorbed oxygen intermediate species during the OER

process. The theoretical overpotential of the OER is defined as $\eta = \max\{(\Delta G1, \Delta G2, \Delta G3, \Delta G4)/e\} - 1.23$ V [50]. The Gibbs free energy diagrams of NiFe LDH and Mn-NiFe LDH are shown in Figs 4 and 5. For pristine NiFe-

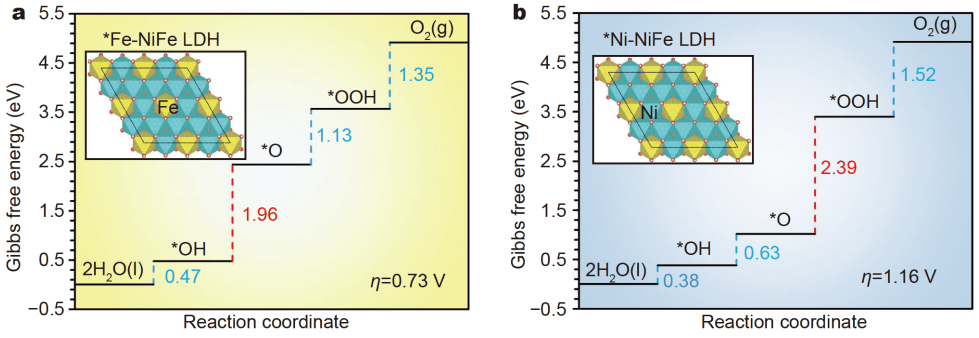

Figure 4 DFT calculations of the Gibbs free energy for NiFe LDH. The Gibbs free energy diagrams of (a) *Fe-NiFe LDH and (b) *Ni-NiFe LDH. The symbol * represents the active sites.

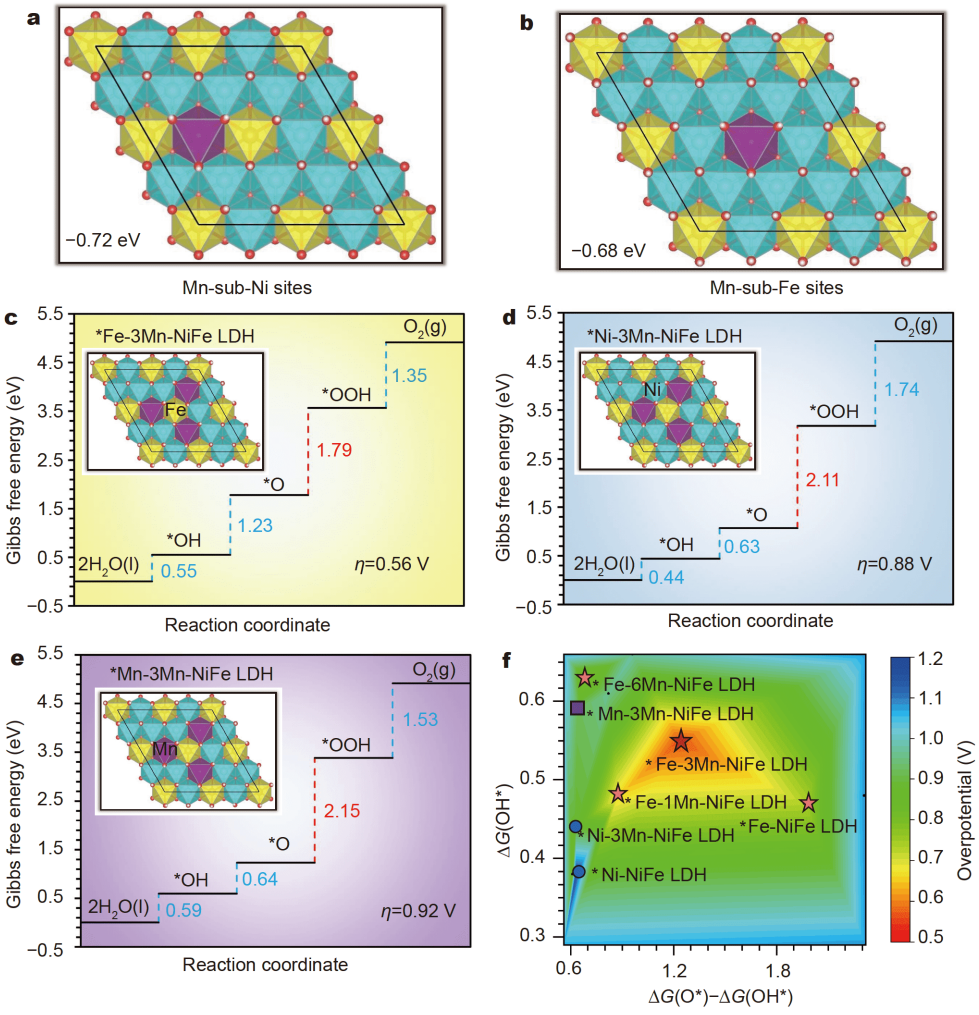

Figure 5 DFT calculations of the Gibbs free energy for Mn-NiFe LDH. The forming energy of (a) Mn-sub-Ni sites and (b) Mn-sub-Fe sites in Mn-NiFe LDH; the Gibbs free energy diagrams of (c) *Fe-3Mn-NiFe LDH, (d) *Ni-3Mn-NiFe LDH, (e) *Mn-3Mn-NiFe LDH and (f) contour plot of theoretical overpotential as a function of ΔG(OH*) and ΔG(O*)−ΔG(OH*). The symbol * represents the active sites.

LDH, the Fe is the major active sites and its potential limiting step is the second step (*OH → *O) with an energy barrier as high as 1.96 eV, providing the high overpotential of 0.73 V (Fig. 4). Specifically, the high overpotential of NiFe LDHs is essentially caused by the weak adsorption of O* on Fe sites. Therefore, strengthening the binding energy of O* is a significant pathway to decrease the overpotential.

Consequently, after Mn substitutes Ni atoms in NiFe LDH (Fig. 5a and b, and Fig. S12), the Gibbs free energy analysis reveals that Fe is still the major active sites and the inherent activity followed the decreasing order of Fe > Mn ≈ Ni (Fig. 5c–e, and Figs S13 and S14). Interestingly, the potential limiting step of Mn-NiFe LDH is switched to the formation *OOH from *O with free energy of 1.79 eV, resulting in the reduced overpotential (η = 0.56 V, Fig. 5c) in comparison with the pristine NiFe LDH (η = 0.73 V, Fig. 4a). This optimal overpotential of 3Mn-NiFe LDH will endow it with excellent OER activity. The above discussion demonstrates that the intrinsic activity can be modulated by introduction of Mn.

Moreover, with the DFT calculation, the relation between the Mn concentration and the OER activity can be completely interpreted. The theoretical calculation reveals that the potential limiting step of Mn-NiFe LDH is the formation *OOH from *O. When the Mn concentration decreases or increases in Mn-NiFe LDH, the Fe active sites exhibit strong adsorption of *O, leading to the high overpotential for OER (Fig. S15 and Table S2).

In order to provide a precise representation map, an overpotential contour plot is provided, which is based on the theoretical activities of metal sites [51,52]. Fig. 5f obviously displays that the central red region (Fe sites) represents the low overpotential in comparison with the border region (Ni and Mn sites). Fe sites on 3Mn-NiFe LDH (near the center of the red region) exhibit moderate binding energies of intermediates, resulting in the excellent OER activity. Benefiting from the overpotential contour plot, one can efficiently adjust the binding energies of oxygen intermediate species by regulating the electronic structures and consequently construct highly active electrocatalysts for water oxidation [53–55].

CONCLUSIONS

In summary, the Mn-doped NiFe LDH/rGO is successfully prepared *via* a simple hydrothermal strategy. The obtained Mn-NiFe LDH/rGO exhibits highly efficient OER activity with a low overpotential (240 mV) to derive 10 mA cm^{-2}, small Tafel slope (40.0 mV dec^{-1}) and remarkable stability in 1.0 mol L^{-1} KOH, which outperforms the NiFe LDH/rGO and RuO_2. The outstanding OER performance of Mn-NiFe LDH/rGO is attributed to the Mn dopant, which efficiently optimizes the electronic structure of the metal active sites, accelerating the OER kinetics. The DFT calculations reveal that Mn with the appropriate concentration in the NiFe LDH/rGO can modulate the adsorption energy of oxygen intermediate species on Fe actives sites and consequently reduce the energy barrier of the rate-determining step. This work provides an effective approach to design highly active and stable OER electrocatalysts of LDH with a potential application in water splitting under alkaline conditions.

Received 4 February 2021; accepted 24 March 2021; published online 22 June 2021

1 Seh ZW, Kibsgaard J, Dickens CF, *et al.* Combining theory and experiment in electrocatalysis: Insights into materials design. Science, 2017, 355: eaad4998
2 Xue Y, Zheng S, Xue H, *et al.* Metal-organic framework composites and their electrochemical applications. J Mater Chem A, 2019, 7: 7301–7327
3 Li P, Zhao X, Duan X, *et al.* A multiphase nickel iron sulfide hybrid electrode for highly active oxygen evolution. Sci China Mater, 2020, 63: 356–363
4 Zhang X, Liu Q, Shi X, *et al.* An Fe-MOF nanosheet array with superior activity towards the alkaline oxygen evolution reaction. Inorg Chem Front, 2018, 5: 1405–1408
5 Cai Z, Bu X, Wang P, *et al.* Recent advances in layered double hydroxide electrocatalysts for the oxygen evolution reaction. J Mater Chem A, 2019, 7: 5069–5089
6 Zhuang L. Ultrathin layered double hydroxide nanosheets with multi-vacancies obtained by plasma technology as oxygen evolving electrocatalysts. Acta Phys Chim Sin, 2017, 33: 1499−1500
7 Ledendecker M, Geiger S, Hengge K, *et al.* Towards maximized utilization of iridium for the acidic oxygen evolution reaction. Nano Res, 2019, 12: 2275–2280
8 Li L, Wang P, Shao Q, *et al.* Metallic nanostructures with low dimensionality for electrochemical water splitting. Chem Soc Rev, 2020, 49: 3072–3106
9 Guo S, Yang Y, Liu N, *et al.* One-step synthesis of cobalt, nitrogen-codoped carbon as nonprecious bifunctional electrocatalyst for oxygen reduction and evolution reactions. Sci Bull, 2016, 61: 68–77
10 Huang L, He Z, Guo J, *et al.* Photodeposition fabrication of hierarchical layered Co-doped Ni oxyhydroxide ($Ni_xCo_{1-x}OOH$) catalysts with enhanced electrocatalytic performance for oxygen evolution reaction. Nano Res, 2020, 13: 246–254
11 Sun K, Zhao L, Zeng L, *et al.* Reaction environment self-modification on low-coordination Ni^{2+} octahedra atomic interface for superior electrocatalytic overall water splitting. Nano Res, 2020, 13: 3068–3074
12 Fu CL, Wang Y, Huang JH. Hybrid of quaternary layered double hydroxides and carbon nanotubes for oxygen evolution reaction. Chin J Struct Chem, 2020, 10: 1807–1816
13 Wang Y, Wang T, Zhang R, *et al.* CuO@CoFe layered double hydroxide core-shell heterostructure as an efficient water oxidation electrocatalyst under mild alkaline conditions. Inorg Chem, 2020, 59: 9491–9495

14 Wu D, Wei Y, Ren X, *et al.* $Co(OH)_2$ nanoparticle-encapsulating conductive nanowires array: Room-temperature electrochemical preparation for high-performance water oxidation electrocatalysis. Adv Mater, 2018, 30: 1705366
15 Ge R, Ren X, Ji X, *et al.* Benzoate anion-intercalated layered cobalt hydroxide nanoarray: An efficient electrocatalyst for the oxygen evolution reaction. ChemSusChem, 2017, 10: 4004–4008
16 Xiong X, Cai Z, Zhou D, *et al.* A highly-efficient oxygen evolution electrode based on defective nickel-iron layered double hydroxide. Sci China Mater, 2018, 61: 939–947
17 Guo M, Zhou L, Li Y, *et al.* Unique nanosheet-nanowire structured CoMnFe layered triple hydroxide arrays as self-supporting electrodes for a high-efficiency oxygen evolution reaction. J Mater Chem A, 2019, 7: 13130–13141
18 Gong M, Dai H. A mini review of NiFe-based materials as highly active oxygen evolution reaction electrocatalysts. Nano Res, 2015, 8: 23–39
19 Yang H, Wang C, Zhang Y, *et al.* Green synthesis of NiFe LDH/Ni foam at room temperature for highly efficient electrocatalytic oxygen evolution reaction. Sci China Mater, 2019, 62: 681–689
20 Yu L, Yang JF, Guan BY, *et al.* Hierarchical hollow nanoprisms based on ultrathin Ni-Fe layered double hydroxide nanosheets with enhanced electrocatalytic activity towards oxygen evolution. Angew Chem Int Ed, 2018, 57: 172–176
21 Jia Y, Zhang L, Gao G, *et al.* A heterostructure coupling of exfoliated Ni-Fe hydroxide nanosheet and defective graphene as a bifunctional electrocatalyst for overall water splitting. Adv Mater, 2017, 29: 1700017
22 Dou Y, He CT, Zhang L, *et al.* How cobalt and iron doping determine the oxygen evolution electrocatalytic activity of NiOOH. Cell Rep Phys Sci, 2020, 1: 100077
23 Stevens MB, Trang CDM, Enman LJ, *et al.* Reactive Fe-sites in Ni/Fe (oxy)hydroxide are responsible for exceptional oxygen electrocatalysis activity. J Am Chem Soc, 2017, 139: 11361–11364
24 Zhang B, Zhu C, Wu Z, *et al.* Integrating Rh species with NiFe-layered double hydroxide for overall water splitting. Nano Lett, 2020, 20: 136–144
25 Xu H, Wang B, Shan C, *et al.* Ce-doped NiFe-layered double hydroxide ultrathin nanosheets/nanocarbon hierarchical nanocomposite as an efficient oxygen evolution catalyst. ACS Appl Mater Interfaces, 2018, 10: 6336–6345
26 Wang TJ, Liu X, Li Y, *et al.* Ultrasonication-assisted and gram-scale synthesis of Co-LDH nanosheet aggregates for oxygen evolution reaction. Nano Res, 2020, 13: 79–85
27 Wang B, Cheng Y, Su H, *et al.* Boosting transport kinetics of cobalt sulfides yolk-shell spheres by anion doping for advanced lithium and sodium storage. ChemSusChem, 2020, 13: 4078–4085
28 Wen L, Zhang X, Liu J, *et al.* Cr-dopant induced breaking of scaling relations in CoFe layered double hydroxides for improvement of oxygen evolution reaction. Small, 2019, 15: 1902373
29 Liu H, Wang Y, Lu X, *et al.* The effects of Al substitution and partial dissolution on ultrathin NiFeAl trinary layered double hydroxide nanosheets for oxygen evolution reaction in alkaline solution. Nano Energy, 2017, 35: 350–357
30 Zhang X, Xu H, Li X, *et al.* Facile synthesis of nickel-iron/nanocarbon hybrids as advanced electrocatalysts for efficient water splitting. ACS Catal, 2016, 6: 580–588
31 Bi Y, Cai Z, Zhou D, *et al.* Understanding the incorporating effect of Co^{2+}/Co^{3+} in NiFe-layered double hydroxide for electrocatalytic oxygen evolution reaction. J Catal, 2018, 358: 100–107
32 Liu S, Lee SC, Patil U, *et al.* Hierarchical MnCo-layered double hydroxides@$Ni(OH)_2$ core-shell heterostructures as advanced electrodes for supercapacitors. J Mater Chem A, 2017, 5: 1043–1049
33 Sun JS, Zhou YT, Yao RQ, *et al.* Nanoporous gold supported chromium-doped NiFe oxyhydroxides as high-performance catalysts for the oxygen evolution reaction. J Mater Chem A, 2019, 7: 9690–9697
34 Chen Z, Zhang Q, Chen W, *et al.* Single-site Au^I catalyst for silane oxidation with water. Adv Mater, 2018, 30: 1704720
35 Chen Z, Chen Y, Chao S, *et al.* Single-atom Au^I-N_3 site for acetylene hydrochlorination reaction. ACS Catal, 2020, 10: 1865–1870
36 Wu K, Sun K, Liu S, *et al.* Atomically dispersed Ni-Ru-P interface sites for high-efficiency pH-universal electrocatalysis of hydrogen evolution. Nano Energy, 2021, 80: 105467
37 Cao E, Chen Z, Wu H, *et al.* Boron-induced electronic-structure reformation of CoP nanoparticles drives enhanced pH-universal hydrogen evolution. Angew Chem Int Ed, 2020, 59: 4154–4160
38 Zhang B, Wang L, Cao Z, *et al.* High-valence metals improve oxygen evolution reaction performance by modulating 3D metal oxidation cycle energetics. Nat Catal, 2020, 3: 985–992
39 Gong M, Li Y, Wang H, *et al.* An advanced Ni-Fe layered double hydroxide electrocatalyst for water oxidation. J Am Chem Soc, 2013, 135: 8452–8455
40 Qin Y, Wang F, Shang J, *et al.* Ternary NiCoFe-layered double hydroxide hollow polyhedrons as highly efficient electrocatalysts for oxygen evolution reaction. J Energy Chem, 2020, 43: 104–107
41 Chen Y, Zhou Q, Zhao G, *et al.* Electrochemically inert g-C_3N_4 promotes water oxidation catalysis. Adv Funct Mater, 2018, 28: 1705583
42 Nadeema A, Dhavale VM, Kurungot S. NiZn double hydroxide nanosheet-anchored nitrogen-doped graphene enriched with the γ-NiOOH phase as an activity modulated water oxidation electrocatalyst. Nanoscale, 2017, 9: 12590–12600
43 Fan K, Chen H, Ji Y, *et al.* Nickel-vanadium monolayer double hydroxide for efficient electrochemical water oxidation. Nat Commun, 2016, 7: 11981
44 Zhong H, Liu T, Zhang S, *et al.* Template-free synthesis of three-dimensional NiFe-LDH hollow microsphere with enhanced OER performance in alkaline media. J Energy Chem, 2019, 33: 130–137
45 He L, Liu J, Liu Y, *et al.* Titanium dioxide encapsulated carbon-nitride nanosheets derived from MXene and melamine-cyanuric acid composite as a multifunctional electrocatalyst for hydrogen and oxygen evolution reaction and oxygen reduction reaction. Appl Catal B-Environ, 2019, 248: 366–379
46 Song F, Hu X. Exfoliation of layered double hydroxides for enhanced oxygen evolution catalysis. Nat Commun, 2014, 5: 4477
47 Ping J, Wang Y, Lu Q, *et al.* Self-assembly of single-layer CoAl-layered double hydroxide nanosheets on 3D graphene network used as highly efficient electrocatalyst for oxygen evolution reaction. Adv Mater, 2016, 28: 7640–7645
48 Liao L, Zhu J, Bian X, *et al.* MoS_2 formed on mesoporous graphene as a highly active catalyst for hydrogen evolution. Adv Funct Mater, 2013, 23: 5326–5333
49 Li Y, Wang H, Xie L, *et al.* MoS_2 nanoparticles grown on graphene: An advanced catalyst for the hydrogen evolution reaction. J Am Chem Soc, 2011, 133: 7296–7299
50 Bajdich M, García-Mota M, Vojvodic A, *et al.* Theoretical investigation of the activity of cobalt oxides for the electrochemical oxidation of water. J Am Chem Soc, 2013, 135: 13521–13530

51 Seitz LC, Dickens CF, Nishio K, *et al.* A highly active and stable $IrO_x/SrIrO_3$ catalyst for the oxygen evolution reaction. Science, 2016, 353: 1011–1014
52 Lu Z, Chen G, Li Y, *et al.* Identifying the active surfaces of electrochemically tuned $LiCoO_2$ for oxygen evolution reaction. J Am Chem Soc, 2017, 139: 6270–6276
53 Kuang M, Zhang J, Liu D, *et al.* Amorphous/crystalline heterostructured cobalt-vanadium-iron (oxy)hydroxides for highly efficient oxygen evolution reaction. Adv Energy Mater, 2020, 10: 2002215
54 Wei YH, Li GS, Wang JH, et al. Self-assembled nanohybrid from opposite charged sheets: Alternate stacking of CoAl LDH and MoS_2. Chin J Struct Chem, 2018, 7: 1093–1101
55 Wang H, Shi G. Layered double hydroxide/graphene composites and their applications for energy storage and conversion. Acta Phys Chim Sin, 2018, 34: 22–35

Acknowledgements This work was supported by the National Natural Science Foundation of China (51902003 and 21771003), Anhui Province Natural Science Foundation (2008085QB53), and the Natural Science Research Project of Anhui Province Education Department (KJ2019A0581).

Author contributions Jiang B, Cheong WC and Wu K designed and carried out the synthesis and characterizations of samples, tested the electrochemical performance, analyzed the data and wrote the manuscript. Tu R, Sun K and Zheng L performed the TEM and XAFS characterization. Liu S analyzed the XAFS data. Shang H and Wang M synthesized the materials. Huang A did the DFT calculations, wrote and revised the manuscript. Wei X revised the manuscript and gave suggestions. Chen C supervised this work.

Conflict of interest The authors declare that they have no conflict of interest.

Supplementary information Experimental details and supporting data are available in the online version of the paper.

Binbin Jiang received his PhD degree from the Institute of Functional Nano & Soft Materials (FUNSOM) of Soochow University in 2018. He has been a lecturer at the School of Chemistry and Chemical Engineering, Anqing Normal University since 2018. His research direction focuses on the field of energy sources.

Weng-Chon (Max) Cheong received his BSc and PhD degrees from the Department of Chemistry, Tsinghua University in 2013 and 2019, respectively, under the direction of Prof. Yadong Li. He is now a lecturer (UM Macao Fellow) at the Department of Physics and Chemistry, University of Macau. His research interests focus on nanosynthesis and electrocatalysis.

Konglin Wu is an associate professor at the School of Chemistry and Chemical Engineering, Anhui University of Technology. He received his PhD degree from the Department of Chemistry at Tsinghua University in 2019 under the supervision of Prof. Yadong Li. His research interest focuses on the design and preparation of single atom, clusters and micro/nanomaterials for energy storage and conversion, and organic catalysis.

Aijian Huang received his BSc degree in electronic information science and technology from the University of Electronic Science and Technology of China (UESTC) in 2018. Currently, he is a PhD candidate at the School of Electronics Science and Engineering, UESTC. His research interests include computer modeling of the electronic, thermal, mechanical, defect and doping properties of semiconductor, catalyst electrode materials with DFT simulation.

Chen Chen received his BSc degree from the Department of Chemistry, Beijing Institute of Technology in 2006, and his PhD degree from the Department of Chemistry, Tsinghua University in 2011 under the direction of Prof. Yadong Li. After postdoctoral work at Lawrence Berkeley National Laboratory with Prof. Peidong Yang, he joined the Department of Chemistry, Tsinghua University as an associate professor in 2015. His research interests focus on nanomaterials and catalysis.

Mn调控NiFe LDH/rGO活性位点的电子结构作为高效水氧化催化剂

江彬彬[1,3†], 张永臻[2,4†], 屠仁勇[2], 孙凯安[2], 柳守杰[5], 吴孔林[1*], 尚恒帅[1], 黄爱鉴[6*], 王淼[1], 郑黎荣[7], 魏先文[1], 陈晨[2*]

摘要 发展廉价、高效的水氧化(OER)催化剂对发展可持续能源具有重要意义. 杂原子掺杂调节活性位点的电子结构提高催化剂的OER性能被认为是一种高效的策略. 本文通过水热法制备得到Mn掺杂的层状镍铁氢氧化物/还原氧化石墨烯(Mn-NiFe LDH/rGO)作为高效、稳定的水氧化催化剂. 实验和模拟计算研究都表明Mn能调整活性位点的电子结构, 改善其对水氧化反应中中间产物的吸附能垒, 从而减小OER反应中决速步骤的反应势垒. 具体而言, 最优的Mn-NiFe LDH/rGO复合材料在过电位仅为240 mV就能驱动10 mA cm^{-2}的电流密度, Tafel斜率低至40.0 mV dec^{-1}, 并且具有良好的稳定性. 该催化剂优异的活性优于最近报道的OER电催化剂. 本工作为制备用于能源转换领域的高活性、廉价的电催化剂提供了新的思路.

